GraphParcelNet: Predicting Parcel-Level Imperviousness from Geospatial Vector Data using Graph Neural Networks

Lapone Techapinyawat
College of Engineering and Computer Science
Texas A&M University – Corpus Christi
Corpus Christi, Texas, USA
ltechapinyawat@islander.tamucc.edu

Wenlu Wang
College of Engineering and Computer Science
Texas A&M University – Corpus Christi
Corpus Christi, Texas, USA
wenlu.wang@tamucc.edu

Mehrube Mehrubeoglu
College of Engineering and Computer Science
Texas A&M University – Corpus Christi
Corpus Christi, Texas, USA
ruby.mehrubeoglu@tamucc.edu

Hua Zhang
College of Engineering and Computer Science
Texas A&M University – Corpus Christi
Corpus Christi, Texas, USA
hua.zhang@tamucc.edu

Abstract

Impervious surfaces increase surface runoff, leading to elevated flood risks and nonpoint source pollution. Predicting impervious surface ratios is essential for various urban management practices, ranging from drainage infrastructure design and water quality assessment to utility fee evaluation and flood risk mitigation. Traditionally, the information on impervious surface ratios is often estimated by city managers and engineers based on empirical values and assumptions. Recent studies have highlighted aerial image classification using machine learning and deep learning models, but such approaches are computationally intensive. We propose a graph neural network (GNN)-driven method, named GraphParcelNet, for advancing the quantification of parcel-level impervious surface ratios at the city scale. To our best knowledge, we are the first to transform land parcel datasets, consisting of vector data in geometric shapes (polygons), into a graph model that considers the spatial relationships between parcels. By utilizing a GNN-based approach, GraphParcelNet enhances the representation of spatial dependencies, resulting in more accurate and reliable predictions over traditional methods. Our experimental results demonstrate that GraphParcelNet outperforms previous methods, providing an accurate measurement for impervious surface ratios.

CCS Concepts

• **Applied computing** → *Earth and atmospheric sciences*; • **Computing methodologies** → **Neural networks**.

Keywords

Graph neural networks, Impervious surface prediction, Geospatial vector data, Land parcel data, Urban infrastructure management

SIGSPATIAL '24, October 29-November 1, 2024, Atlanta, GA, USA

ACM ISBN 979-8-4007-1107-7/24/10
https://doi.org/10.1145/3678717.3691281

ACM Reference Format:
Lapone Techapinyawat, Wenlu Wang, Mehrube Mehrubeoglu, and Hua Zhang. 2024. GraphParcelNet: Predicting Parcel-Level Imperviousness from Geospatial Vector Data using Graph Neural Networks. In *The 32nd ACM International Conference on Advances in Geographic Information Systems (SIGSPATIAL '24), October 29-November 1, 2024, Atlanta, GA, USA.* ACM, New York, NY, USA, 11 pages. https://doi.org/10.1145/3678717.3691281

1 Introduction

Rapid urbanization transforms natural landscapes into impervious surfaces, which do not allow precipitation to infiltrate the ground, causing increased surface runoff accumulation [24, 32]. In contrast, pervious surfaces, such as grass and soil, permit the infiltration of precipitation. In land parcels within urban environments, major impervious areas include roofs and driveways, as shown in Figure 1. Densely populated areas see an increase in impervious surfaces, significantly impacting stormwater management. Engineers must manage runoff to prevent flooding, making impervious surface ratios essential for various management strategies. These strategies range from drainage infrastructure design and water quality assessment to utility fee evaluation and flood risk analysis.

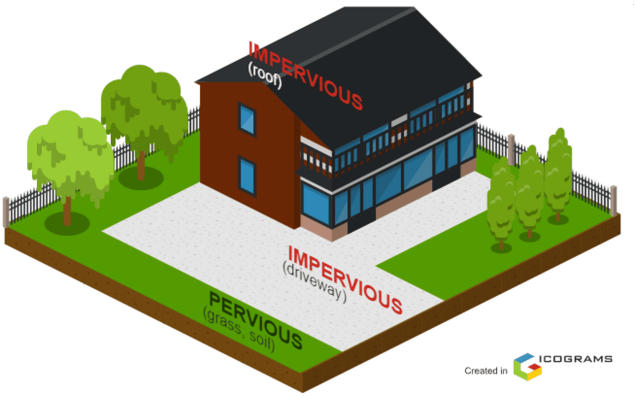

Figure 1: Major components of land cover in a land parcel, illustrating impervious surfaces (roof, driveway) and pervious surfaces (grass, soil).

Accurate assessment of impervious surfaces benefits hydrological modeling, improves stormwater management practices, and ensures that property owners are charged fairly according to their runoff contribution [16]. Thus, precise measurement of impervious surfaces is crucial for environmental protection and sustainable urban planning [13].

Deep learning has significantly advanced geospatial variable estimation, with convolutional neural networks (CNNs) being widely used to analyze satellite images. These networks have proven effective in predicting various geospatial data, including socioeconomic metrics like median income levels [6]. Additionally, CNNs can integrate specialized layers, such as spatial pyramids, to improve model predictions [10, 17]. In urban analysis, CNNs have been employed to classify land cover from high-resolution aerial or satellite imagery, identifying and categorizing each pixel into different land cover types, such as impervious surfaces, vegetation, or water. This pixel-based approach, as demonstrated in previous work [25], generates detailed land cover data across large areas. These land cover data can then be used to estimate impervious surface ratios by calculating the proportion of impervious pixels within each land parcel. While highly accurate, this method requires substantial computational resources, particularly when applied to large urban areas. Traditional pixel-based deep learning techniques on satellite images are often resource-intensive [1, 14, 28]. The use of high-resolution imagery, coupled with the need for labor-intensive labeling and substantial computational power for large-scale tasks, poses challenges to the efficiency and scalability of these methods [31].

Given the resource demands of pixel-based deep learning techniques, it is crucial to explore alternative approaches for spatial analysis in a shift toward vector domain analysis. One promising solution is the use of Graph Neural Networks (GNNs), introduced in 2009 [22]. Unlike traditional deep learning methods that rely on predefined tables, GNNs represent data relationships as graphs. This allows GNNs to model complex interactions and offers significant flexibility for structural analysis tasks. They have been successfully applied in various fields, including chemical reactions, text sequences, and image classification [34]. In urban geospatial datasets, GNNs can effectively represent spatial relationships through graph structures rather than tabular datasets. This approach aligns with Tobler's First Law of Geography, which states that entities closer in space exhibit stronger correlations [27]. The proximity of nodes in a graph can indicate more significant connections, making graphs formed from spatial interrelations more relevant for evaluating impervious surfaces than conventional non-spatial, tabular datasets.

We propose GraphParcelNet, a graph neural network designed to predict variables of land parcels, specifically impervious surface ratios in urban environments. To leverage the spatial relationships between land parcels, node features are created directly from land parcel centroids, utilizing 40 diverse variables, including land cover information (spectral index statistics) and demographic characteristics. Edges in the graph are established through Delaunay triangulation, utilizing Euclidean distances between centroids to enrich the dataset with spatial context. This approach offers an alternative to traditional deep learning techniques of image classification and tabular regression for parcel-level feature prediction.

The following summarizes our contributions:

- Our proposed method uses vector domain features, which require substantially lower spatial resolution and lower computational complexity compared to the raster domain classification used in traditional land cover analysis, which relies heavily on substantial storage and computational resources.
- To our best knowledge, we are the first one to propose a graph construction from land parcel data: Constructing a graph from land parcel data using centroid areas and Delaunay triangulation to capture spatial interrelations more effectively. Our GraphParcelNet considers spatial dependencies that are superior to previous methods.
- We comprehensively assess the model's performance using different architectures and compare it to various previous models, along with a full ablation study.

The paper is structured as follows: Section 2 provides an overview of related work, including traditional methods. In Section 3, the proposed model, GraphParcelNet, is described in detail, including its architecture and the integration of graph construction for geospatial vector data. This section explains how land parcel data is transformed into a graph structure and details the specifics of our proposed GraphParcelNet. Section 4 describes the dataset and study area, baseline models, evaluation results, ablation study, hyperparameter tuning, and the impact of training sample size on regression accuracy. Lastly, Section 5 summarizes the conclusions from our study.

2 Related work

Impervious surface ratios are the primary input for various management strategies, ranging from drainage infrastructure design and water quality assessment to utility fee evaluation and flood risk analysis. Traditionally, the information on the impervious surface ratios is often estimated by city managers and engineers based on empirical values and assumptions. Recent studies have highlighted aerial image classification using deep learning and machine learning to determine land cover, a common approach in the raster domain. This method involves classifying each pixel in the image as either impervious or pervious, as illustrated in Figure 2. The impervious ratio for each parcel is then calculated by summing the impervious pixels and dividing by the total number of pixels in the parcel. However, this method is resource-intensive and computationally demanding. There is potential to estimate the impervious surface ratio using alternative approaches, primarily in the vector domain. In traditional machine learning and deep learning models, regression tasks are typically performed using models such as TabNet, Multi-Layer Perceptron (MLP), Support Vector Regression (SVR), and CatBoost. These models perform exceptionally well in general applications. TabNet utilizes a sequential attention mechanism to handle data, excelling in feature-rich datasets [2]. MLP and SVR are widely used for their simplicity and effectiveness [19], while CatBoost, a gradient boosting algorithm, manages overfitting effectively [20]. However, these models typically start with tabular data (such as DataFrame in Python), where samples are listed in rows without any spatial linkage between them. This lack of spatial connection between samples limits their potential benefits in geospatial data analysis. Consequently, exploring graph-based approaches that can leverage spatial relationships between land

parcels presents a promising direction for improving impervious surface ratio estimation.

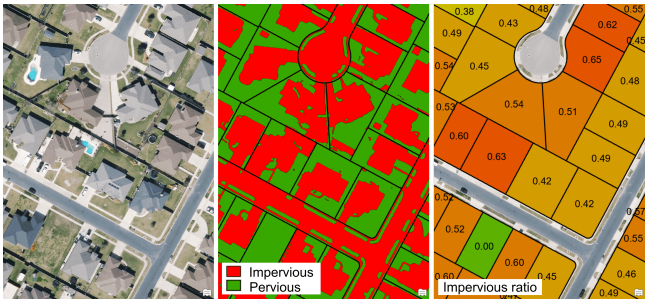

Figure 2: Recent method for quantifying impervious surface ratio. The process involves classifying each pixel in aerial imagery as impervious (red) or pervious (green) and calculating the ratio of impervious pixels within each land parcel.

To enhance the spatial relationships between samples in geospatial data, deep learning analysis can be performed using graph input features in Graph Neural Networks (GNNs). GNNs offer unique advantages by leveraging graph structures to represent data, capturing complex relationships such as distance and adjacency that are difficult to model with traditional methods. Several GNN architectures, such as Graph Convolutional Networks (GraphConv) and Graph Isomorphism Networks (GIN), are explicitly designed to handle spatial relationships in their tasks. GraphConv, introduced in 2017, convolves information from neighboring nodes to update a node's representation [18]. This method has demonstrated strong performance across various research fields, ranging from molecular scale studies to social network analyses [4, 7]. It effectively captures spatial relationships between nodes in a graph, performing well in general graph learning tasks where these relationships are crucial. However, GraphConv struggles with isomorphic graphs, where identical structures have different node orders. GIN, introduced in 2019, addresses the limitations of GraphConv by prioritizing the distinction of isomorphic graphs through a unique aggregation mechanism [33]. This makes GIN beneficial for tasks involving isomorphic graphs where order independence is essential.

Building on the strengths of GNN architectures, innovative frameworks have been developed to solve geospatial analysis in urban environments. For example, Spatial Regression Graph Convolutional Neural Networks (SRGCNNs) integrate spatial regression techniques with GNNs, capturing complex urban features by incorporating diverse datasets such as social media check-ins and real estate values [35]. Multigraph convolutional networks further extend GNN capabilities by managing multiple relationships between nodes, supporting comprehensive regional economic performance analysis [12]. Additionally, Positional Encoder Graph Neural Networks enhance GNNs' ability to process geographic data by embedding positional encodings alongside traditional node features, which is essential for land use classification and environmental monitoring [15]. These models demonstrate the promise of geospatial analysis and highlight the potential for GNNs to predict various variables at the land parcel level, an innovative approach that has not been extensively explored.

To address the limitations of conventional impervious surface ratio estimation through image classification, exploring the use of GNNs in geospatial data analysis in a regression approach at the land parcel level offers a promising alternative. The application of GNNs for predicting impervious surface ratios at the land parcel level represents a novel and underexplored direction in geospatial analysis, capturing spatial relationships between parcels that existing regression methods could not represent. This shift not only improves estimation accuracy over existing regression models but also opens new avenues for advanced urban planning and environmental management.

3 Proposed method

This study employs a GraphConv model to predict the impervious surface ratios at the land parcel level, focusing on uncovering complex spatial relationships between parcels based on location and distance. Traditional machine learning and deep learning models typically process training data in tabular form, which cannot incorporate spatial context. The development of the GraphParcelNet model comprises two primary phases: Graph construction and Graph Neural Network (Figure 3).

3.1 Graph Construction

In Phase 1, the process begins with gathering input features for training the GNN. These features come from spectral indices obtained from aerial imagery and demographic data from the American Community Survey (ACS) zonal statistics. The method uses these inputs to construct a graph-structured dataset for the GNN. The proposed GraphParcelNet approach diverges from traditional pixel classification methods that classify land cover types pixel by pixel using a raster dataset. Instead, it uses an input vector dataset, enabling faster and less resource-intensive prediction of the impervious surface ratios at the land parcel level. Both raster and vector data are suitable for constructing input features. A zonal statistical analysis, including mean, median, standard deviation, minimum and maximum pixel values, range, summation, and spectral index percentiles, represents each parcel with a singular value. If the feature data is already in vector form, such as demographic data, it can be used directly without statistical processing.

In this study, we define the parcel system as a graph $G = (N, E)$, where $N = \{n_1, ..., n_N\}$ represents a set of nodes corresponding to individual parcels, and E denotes a set of undirected edges that capture spatial relationships (adjacency and distance) between these parcels. To construct the graph-structured data for the deep learning model (Figure 3), the method imports the shapefile of land parcels, which includes field values as input features.

The shapefile is transformed into a GeoDataFrame, and the numeric features are normalized using a standard scaling procedure across the global dataset, which encompasses all data points. Specifically, a minimum-maximum scaling method is applied to normalize features to a fixed range of -1.0 to 1.0. This method adjusts the minimum and maximum values of each feature to ensure that all features contribute equally to the model training process, preventing any single feature from dominating. After normalization, the global dataset is divided into training, validation, and testing subsets. The scaling parameters derived from the global dataset are then applied

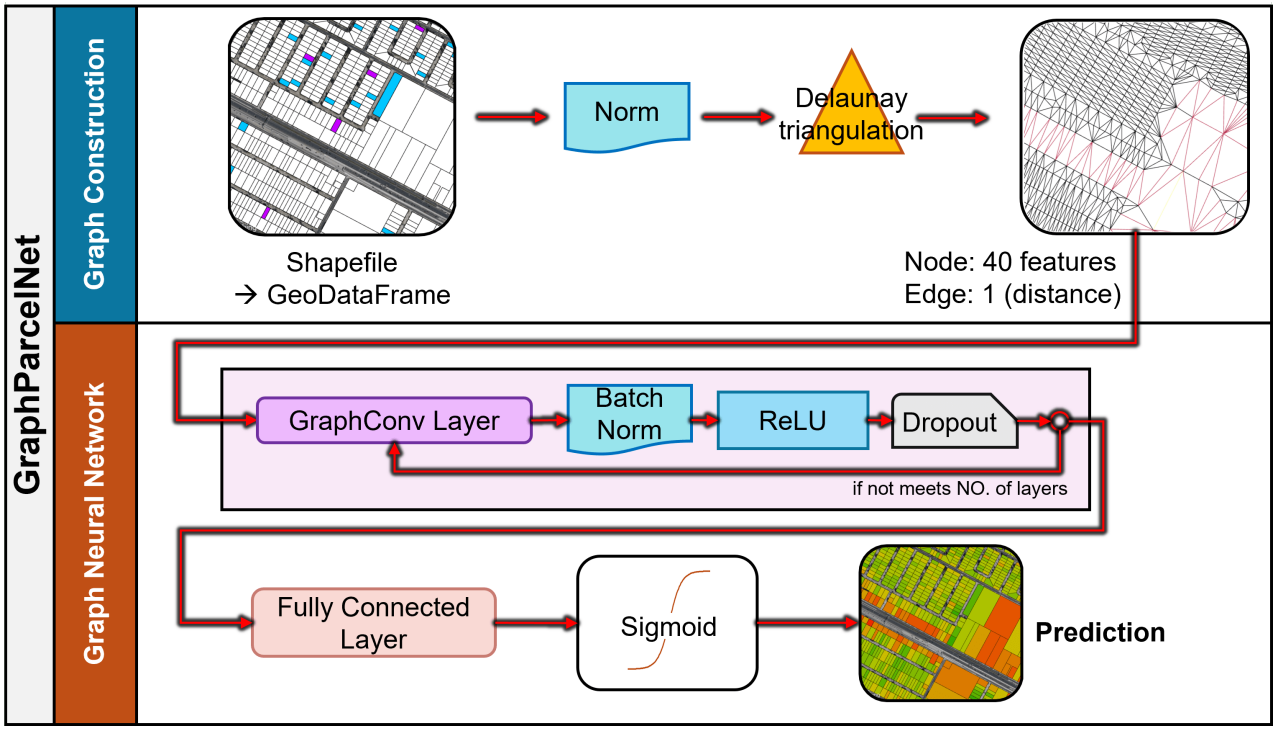

Figure 3: The proposed GraphParcelNet framework.

uniformly to these subsets. Each subset is configured into a graph structure for input into the GNN model. The centroid area method defines the features of each land parcel node. The graph structure is constructed using the Delaunay triangulation method [3], with the distances between connected nodes serving as edge features. The steps of the graph construction are shown in Algorithm 1.

Algorithm 1 Graph Construction

Require: global_data, train_data, valid_data, test_data
Ensure: train_graph, valid_graph, test_graph
1: Load global_data for Normalization
2: Read global shapefile and fit MinMaxScaler.
3: Normalize Numeric Features in Data
4: **for** *data* in {train_data, valid_data, test_data} **do**
5: Identify and normalize numeric input features, excluding the target feature "Impervious ratios", using the fitted *scaler*.
6: Extract centroids of shapes in *data* to form *points*.
7: Create Delaunay triangulation from *points*.
8: Extract edges from the triangulation and store in *edge_structure*.
9: Calculate Euclidean distances as *edge_attributes*.
10: Create data objects with normalized features, edges, edge attributes, and labels.
11: **end for**
12: Return *train_graph*, *valid_graph*, and *test_graph*.

3.2 Graph Neural Network

Phase 2 focuses on the graph neural network architecture following graph construction (Figure 3). This study employs a GraphConv model to capture the complex relationships present in geospatial datasets. The input layer starts with the graph created in Phase 1. The GraphConv model is particularly suitable for this task because it can aggregate information from neighboring nodes, allowing for effective modeling of dependencies between parcels. This aggregation mechanism involves summing the features of neighboring nodes to update each node's feature representation. This process ensures that each node's features are influenced by its surrounding nodes, effectively capturing the characteristics of neighboring parcels. The GraphConv model uses the following equation to update node features:

$$\text{GraphConv}(H^{(k)}) = \tilde{D}^{-1/2}\tilde{A}\tilde{D}^{-1/2}H^{(k)}W^{(k)}$$

where $H^{(k)}$ represents the node features at layer k, $\tilde{A}$ is the adjacency matrix derived from Delaunay triangulation, $\tilde{D}$ is the degree matrix, and $W^{(k)}$ are the trainable weight matrices.

The output from the prediction layer is processed through a residual block that includes ReLU activation, batch normalization, and dropout. The output layer then either returns to the GraphConv layer or proceeds to a fully connected layer, depending on the number of specified GraphConv layers. If the number of GraphConv layers is more than one, the graph undergoes another aggregation mechanism. Otherwise, the GNN process is complete, and the output proceeds to the fully connected layer. This single-channel output is then passed through a sigmoid function, the final function

before obtaining the impervious surface ratios prediction, to ensure that the values remain within the 0.00 to 1.00 range, which is the domain for the impervious surface ratios.

$$\mathrm{DBN}(H) = \mathrm{Dropout}(\max(0, \mathrm{BN}(H)), p)$$

$$\hat{y} = \sigma(W^{final} H^{last})$$

where p is the dropout rate and σ is the sigmoid function.

A loss function based on the mean absolute error (MAE) method is utilized to optimize the model's predictions. The GNN framework is described by the following mathematical equation:

$$\mathrm{GNN} = \sigma\left(\mathrm{DBN}(\mathrm{GraphConv}(H^{(k)}))\Big|_{k=1}^{n}\right)$$

where k represents the layer index, n is the total number of layers, σ is the sigmoid function, and DBN denotes the dropout and batch normalization applied to the output of the GraphConv layer.

To conclude, the GraphParcelNet framework is structured in two primary phases: Graph Construction and the application of the GNN model.

4 Experiments

4.1 Datasets

The experimental component of this study was conducted in Corpus Christi, Texas, USA. Node features were determined using statistical measures of various spectral indices obtained from multispectral aerial images, representing surface characteristics of individual land parcels. These indices were calculated using formulas that combined different spectral bands to emphasize particular features. For instance, the Normalized Difference Vegetation Index (NDVI) measured vegetation health and vigor [11]. Similarly, the Normalized Difference Water Index (NDWI) indicated moisture content [5]. The Modified Triangular Vegetation Index 2 (MTVI2) and Visible Atmospherically Resistant Index (VARI) were used to assess vegetation cover [8, 9].

Demographic data for block groups from the Environmental Justice Screening and Mapping Tool provided by the United States Environmental Protection Agency (EPA) supplemented the non-raster dataset [29, 30]. Land parcel information was obtained from the Texas Geographic Information Office (TxGIO), delineating individual parcel blocks as shown in Figure 4 [26]. Table 1 lists the 40 node features extracted from aerial images and demographic data. The target feature for the model was the impervious surface ratio within each parcel block, ranging from 0.00-1.00.

After cleaning the data, the total number of parcel blocks within the study area remained at 103,828. A subset of 5,000 parcels was used for model training, and an additional 1,000 parcels were reserved for validation to assess its generalization capacity, as depicted in Figure 5. The test set comprises the remaining 97,828 parcels.

4.2 Baselines

All input features for the baseline models were in tabular format (DataFrame). Before the training and validation steps, these features were normalized using the same approach as our proposed GraphParcelNet model to ensure a fair comparison. The training,

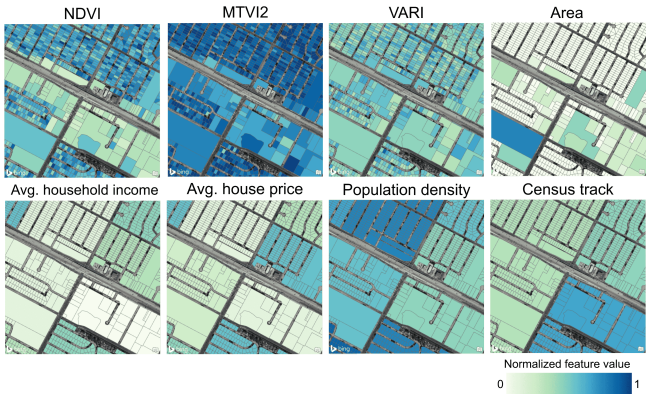

Figure 4: Examples of input features from spectral indices and demographic data.

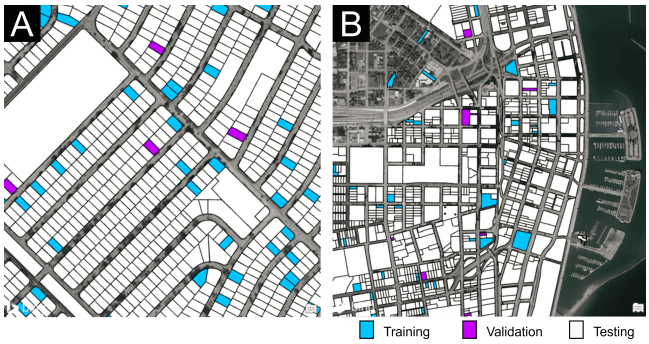

Figure 5: Distribution and density of the training, validation, and testing datasets.

validation, and testing datasets comprised 5,000, 1,000, and 97,828 samples, respectively. All models used the same MAE loss function for training and validation.

TabNet [2], MLP, SVR [19], and CatBoost [20] baseline models were used as benchmarks against the GraphParcelNet, providing a benchmark for evaluating the impervious surface ratio predictions. These models were selected to utilize their respective strengths, enhancing the overall accuracy and reliability of impervious surface ratio estimation. There are two sets of evaluation results: one from the validation (1,000) phases during model training and another from the test phase (97,828). Our study used results from a previous study of the exact same area, derived from pixel classification of 15-cm resolution aerial imagery, considered the most reliable method (ground truth) for this study as it quantifies land cover to compare regression errors. The validation results were evaluated based on metrics of MAE loss and mean square error (MSE).

The testing results were evaluated using two groups of metrics. The first group includes metrics where a lower value indicates better performance: MAE, MSE, median absolute error (Median AE), quantile loss, Earth Mover's Distance (EMD), and Kolmogorov-Smirnov Statistic (KS Statistic) [21, 23]. The second group includes metrics where values closer to the ground truth indicate better performance: minimum, maximum, mean, median, standard deviation,

Table 1: Node features and their descriptions.

Features	Variants	Description
NDVI	Mean, Std, Min, Max, Range, Sum, Median, Pct90	Vegetation index derived from the visible and near-infrared light reflected by vegetation.
NDWI	Mean, Std, Min, Max, Range, Sum, Median, Pct90	Water index for moisture/liquid water content of soil and vegetation.
MTVI2	Mean, Std, Min, Max, Range, Sum, Median, Pct90	Enhanced vegetation index to correct soil and atmosphere influences.
VARI	Mean, Std, Min, Max, Range, Sum, Median, Pct90	Index for visualizing vegetation in RGB imagery.
Demographics	Census track, Population density, Average home price, Average family income	Demographic information at block group level.
Coordinates	X, Y	Projected coordinates of the parcel.
Shape	Length, Area	Geometric measurements of the parcel shape.

mode, interquartile range (IQR), skewness, kurtosis, and coefficient of variation (CV). These evaluation metrics were used to highlight the ability of the GNN to capture its own errors and prediction density distribution compared to the pixel classification (ground truth), which is expected to outperform the baseline models in predicting impervious surface ratios.

4.3 Evaluation

The optimal model configuration, identified after testing 72 combinations of 4 hyperparameters, comprised a learning rate of 0.001, two GraphConv layers, a hidden dimension of 128, a dropout rate of 0.5, and a weight decay of 0.00001. Averaged across 10 iterations during training, this configuration yielded a training loss of 0.0486, a validation loss of 0.0548, and a MSE of 0.0070. The CatBoost model, the most competitive baseline, had a larger validation MAE loss of 0.0573 but a slightly lower MSE loss of 0.0065. Other baseline model performances are detailed in Table 2.

For the testing dataset evaluation, two groups of metrics were used, as presented in Table 3 and 4. Overall, the metrics indicate that the GraphParcelNet model performs better than the baseline models regarding minimum, maximum, standard deviation, mode, interquartile range, kurtosis, coefficient of variation, MAE, median absolute error, quantile loss, Earth Mover's Distance, and Kolmogorov-Smirnov Statistic. These metrics suggest a better overall alignment of the predicted distributions with the ground truth. Notably, the minimum, maximum, and mode metrics capture how well the model can estimate the ratio and identify common ratios. EMD measures the minimal cost to transform one distribution into another, while KS measures the maximum distance between empirical cumulative distribution functions.

Table 2: Training and Validation Results

Model	Validation Loss MAE	Validation MSE
TabNet [2]	0.0806	0.0114
MLP [19]	0.0731	0.0096
SVR [19]	0.0732	0.0093
CatBoost [20]	0.0573	<u>0.0065</u>
GraphParcelNet	<u>0.0548</u>	0.0070

The comparison of the testing dataset between the GraphParcelNet model, the baseline models (TabNet, MLP, SVR, and CatBoost), and a pixel classification method (considered the ground truth for this study) revealed distinct probability density functions of predicted impervious surface ratios (Figure 6a). The pixel classification method demonstrated a broad spectrum of impervious surface ratios, particularly at the boundary values, indicating regions with no impervious surfaces (value of 0), such as undeveloped parcels, and entirely impervious areas (value of 1), such as downtown high-rises. The GraphParcelNet model effectively captured these boundary conditions, especially the impervious surface ratios of 0, which closely aligned with the ground truth. While the ratios of 1.00 were slightly overestimated, GraphParcelNet's mode statistic indicated that the most common impervious surface ratios of land parcels were similar to the ground truth. Additionally, GraphParcelNet's mode density was the best among the baseline models.

CatBoost, the most competitive baseline model as illustrated presented in Table 3 and 4, showed a high density of estimated impervious surface ratios below the mode of the ground truth, and its density was significantly higher than that of the ground truth. However, the shape of CatBoost's plot did not align with the ground truth, exhibiting unrealistic patterns. Although CatBoost captured the ratios at the boundary condition of 0.00, it tended to underestimate them and struggled with ratios at 1.00, often shifting towards 0.95.

The remaining baseline models predicted the impervious surface ratios but were not as effective as GraphParcelNet, particularly at the boundary conditions of 0.00 and 1.00. For instance, some agricultural lands were predicted to have certain impervious ratios, or fully developed lands such as buildings and parking lots were incorrectly quantified as less than 100% impervious. The ability to capture these extreme values is crucial because they affect stormwater management practices and the assessment of stormwater fees. Additionally, model predictions should ideally remain within the range of 0.00 to 1.00 since they represent ratios. Models such as TabNet, MLP, and SVR, which produced predictions significantly outside this range, demonstrated weaker performance in this context. Ensuring that predictions fall within the expected range indicates a model's accuracy.

In terms of residual error, GraphParcelNet produced less residual error than CatBoost. The probability density plot (Figure 6b)

Table 3: Testing Results: Lower value indicates better performance. MAE: Mean Absolute Error, MSE: Mean Squared Error, Median AE: Median Absolute Error, EMD: Earth Mover's Distance, KS Statistic: Kolmogorov-Smirnov Statistic

Model	MAE	MSE	Median AE	Quantile Loss	EMD	KS Statistic
TabNet [2]	0.0817	0.0191	0.0603	0.0408	0.0332	0.0897
MLP [19]	0.0737	0.0114	0.0545	0.0368	0.0244	0.0507
SVR [19]	0.0728	0.0099	0.0552	0.0364	0.0242	0.0474
CatBoost [20]	0.0573	0.0070	0.0417	0.0286	0.0174	0.0585
GraphParcelNet	0.0573	0.0078	0.0394	0.0286	0.0072	0.0228

Table 4: Testing Results: Closer value to ground truth indicates better performance. Min: Minimum, Max: Maximum, Std: Standard Deviation, IQR: Interquartile Range, CV: Coefficient of Variation. † Ground truth is based on pixel classification.

Model	Min	Max	Mean	Median	Std	Mode	IQR	Skewness	Kurtosis	CV
TabNet [2]	-1.07	11.33	0.435	0.398	0.205	0.307	0.2348	5.8559	218.2504	0.4715
MLP [19]	-0.73	3.99	0.431	0.410	0.207	0.344	0.2317	0.8975	5.4478	0.4806
SVR [19]	-0.65	1.51	0.424	0.404	0.201	0.380	0.2422	0.5488	0.9637	0.4730
CatBoost [20]	-0.04	1.03	0.429	0.398	0.210	0.338	0.2492	0.4394	0.3579	0.4899
GraphParcelNet	0.00	1.00	0.428	0.410	0.227	0.425	0.2524	0.4803	0.2849	0.5304
Ground truth†	0.00	1.00	0.424	0.413	0.224	0.425	0.2592	0.3884	0.1404	0.5295

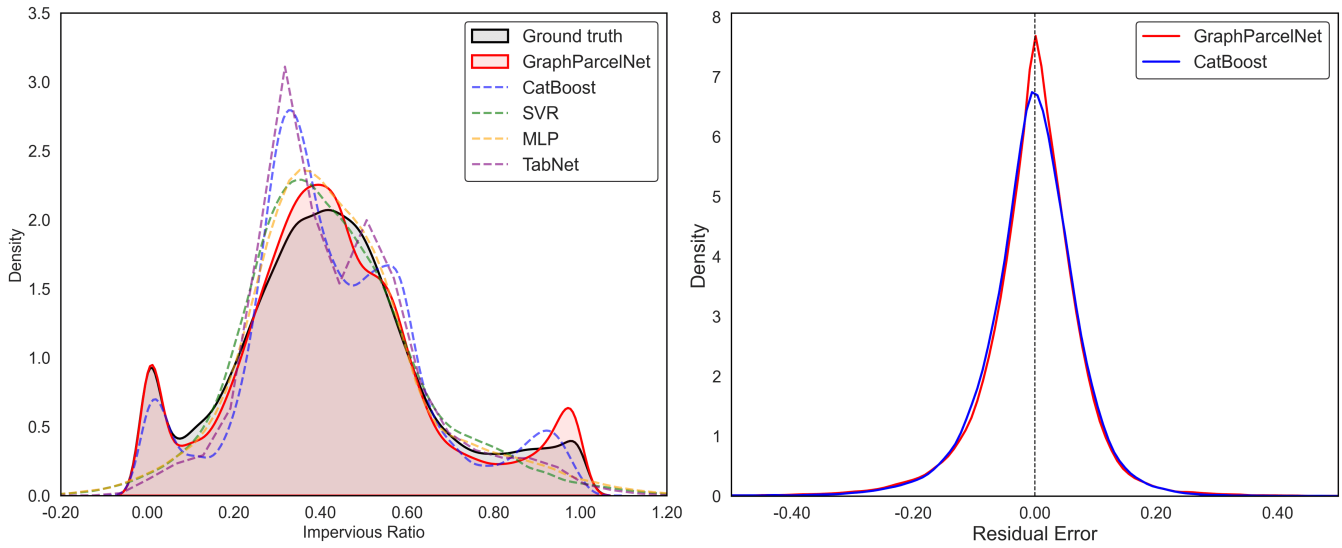

Figure 6: (a) Probability density functions of predicted impervious surface ratios compared to ground truth for GraphParcelNet, CatBoost, SVR, MLP, and TabNet models. The ground truth derived from pixel classification; (b) Probability density plot of residual errors for GraphParcelNet and CatBoost.

showed that GraphParcelNet had a higher peak (density) at a residual error of 0.00, indicating more accurate predictions with less error compared to CatBoost. Ideally, a perfect prediction model would show a spike at a residual error of 0.00. However, both regression models still produced errors within a range between -15% and +15%, with overestimations and underestimations occurring equally, as shown by the systematic plots. Overall, GraphParcelNet outperformed the baseline models in predicting impervious surface ratios.

Figure 7 provided illustrated the spatial comparative analysis for urban landscape characterization. Example 1 demonstrated the capabilities of GraphParcelNet and CatBoost in capturing high impervious surface ratios in commercial zones along business corridors and major roads. The satellite image showed that these commercial stripes consisted of large buildings and expansive parking lots, which should have higher impervious surface ratios than residential zones. Both GraphParcelNet and CatBoost captured this scale well.

Example 2 showed that both models could predict the imperviousness of residential areas with detached houses and apartments

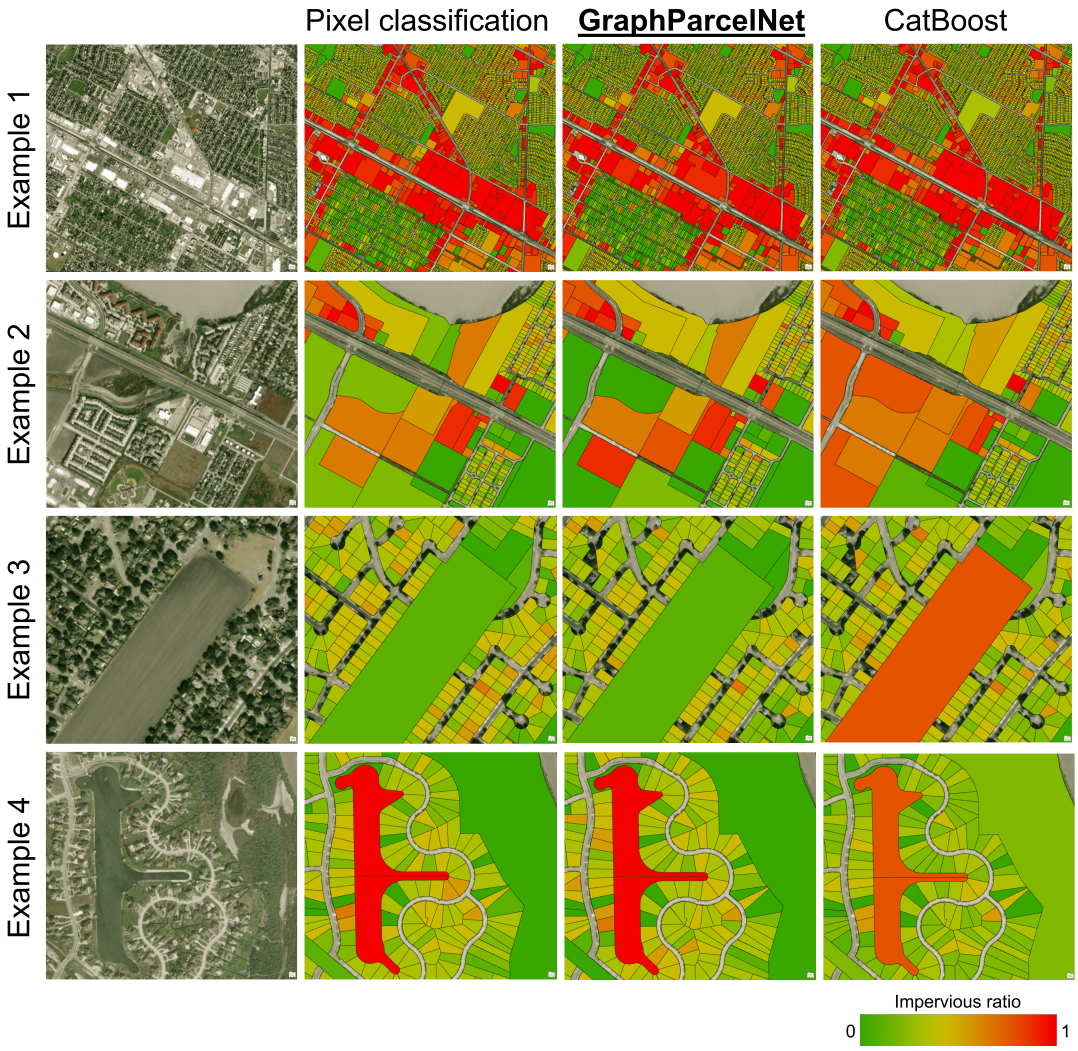

Figure 7: Testing dataset predictions highlighting the GNN model's spatial discernment.

accurately. However, CatBoost sometimes mistakenly predicted large parcels, such as undeveloped land and agricultural land, as having high impervious ratios. In this example, CatBoost predicted the undeveloped parcels (dark orange) with higher impervious ratios, which should have been green. Furthermore, CatBoost predicted these undeveloped parcels as having higher impervious ratios than the apartment complex parcel (light orange).

Example 3 further illustrated that CatBoost predicted that the undeveloped parcel in the middle of the figure would have a high impervious ratio, higher than all surrounding residential neighborhoods, which was unrealistic. This incorrect prediction was further problematic due to the parcel's large size. If this prediction existed in hydrological modeling, such errors could significantly impact model accuracy.

Lastly, Example 4 depicted a retention pond in a residential neighborhood. This water body considered impervious due to low infiltration capability, should have had an impervious ratio of 1.00. GraphParcelNet predicted it correctly, whereas CatBoost predicted slightly lower than 1.00, as shown in light orange. This low ability of CatBoost to capture impervious ratios of 1.00 was indicated in the probability plot in Figure 6a. These examples highlighted the superior performance of GraphParcelNet over CatBoost in predicting impervious surface ratios at detailed scales.

4.4 Ablation Study

The proposed GraphParcelNet framework utilized the Delaunay triangulation method to construct a graph from land parcel centroids. However, alternative algorithms, such as the K-nearest neighbors algorithm, can construct graphs based on different principles by linking each centroid to its closest neighbors. To evaluate the efficacy in terms of time, memory usage, and predictive performance, we compared the K-nearest neighbors algorithm with configurations of 10, 20, and 100 nearest neighbors against the Delaunay method and a pixel classification method using 15-cm resolution

aerial imagery with Deeplabv3+ and a ResNet 101 backbone from a previous study [25]. The pixel classification method used in that study, which focused on generating land cover data, was used here to compare its results to the vector-based regression model introduced in this paper. All computations were performed on a system equipped with an Intel Xeon Silver 4214R CPU at 2.40 GHz, 32 GB of RAM, and an NVIDIA RTX A4000 GPU.

As shown in Table 5, Delaunay triangulation yielded the best results compared to other vector domain models, with the fastest graph construction time and lowest memory usage, followed by the 10 and 20 nearest neighbors methods. The 100 neighbors method utilized the most memory. During the training and validation process, which involved up to 4000 epochs, the Delaunay method required the least time and memory. Increasing the number of neighbors significantly raised computation time without improving predictive performance, as indicated by higher error metrics. During testing, time usage varied slightly across methods but remained within a range of seconds, with Delaunay triangulation consistently showing the lowest errors.

In contrast to these findings, the previous study [25] focused on generating accurate land cover data with several surface types, not impervious ratios, using a pixel-based approach. The results of that study could then be used to estimate impervious surface ratios within parcels. The current study addresses the efficiency challenges by predicting impervious surface ratios directly within the vector domain using a novel GNN-based approach. Table 5 also highlights that the proposed method for estimating impervious surface ratios using a vector domain regression model was significantly faster than pixel classification, taking less than 2 seconds for the entire 312 km² study area, compared to 122 hours for pixel classification. This demonstrates the practicality and efficiency of GraphParcelNet in comparison to pixel classification.

4.5 Hyperparameter tuning

Hyperparameters were selected for the GNN model to optimize predictive performance, as outlined in Table 6. The learning rate was tested at 0.001, 0.0001, and 0.00001. The model's depth, specified by the number of GNN layers, was adjusted between one and four iterations. The hidden dimension values tested were 32, 64, and 128 units to determine the complexity required for capturing patterns in the data. Dropout rates of 0.5 and 0.8 were applied to perform generalization. Weight decay was set at 0.00001 to prevent overfitting. The maximum number of epochs was established at 4000.

A comprehensive hyperparameter tuning process was conducted, and the 72 results are summarized in Figure 8. The learning rate had a notable impact on model performance, with lower learning rates resulting in higher validation loss. Similarly, an increase in dropout rate correlated with increased loss, indicating reduced model generalization. The effect of the number of layers on loss exhibited some variability, but generally, deeper models tended to incur higher losses. Conversely, variations in the hidden dimension had a relatively minor impact on the loss, suggesting that the model's capacity was not significantly influenced by the size of the hidden dimensions.

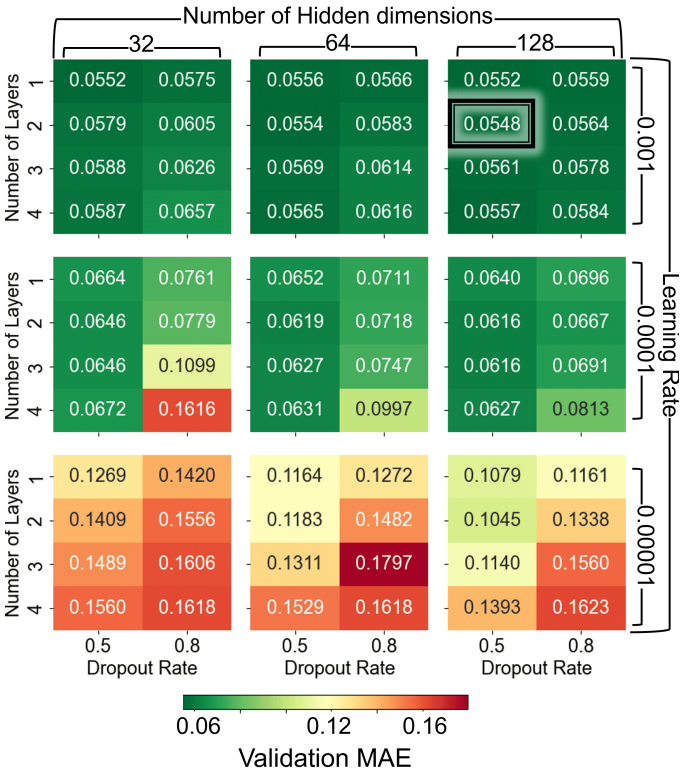

Figure 8: Validation MAE for different combinations of hyperparameters in the GraphParcelNet model.

4.6 Impact of training sample size on regression accuracy

Increasing the number of training samples potentially increased the accuracy of deep learning models; however, this came at the cost of a more significant time investment to achieve a satisfactory error rate. Despite the training dataset comprising less than 5% of the total parcels (5,000 out of 102,828), acquiring accurate ground truth values for these 5,000 samples posed a significant challenge. The analysis investigated how the number of training samples affects the model prediction performance, with each set undergoing 10 iterations to determine average performance. The analysis covered six training dataset sizes: 10, 50, 100, 500, 1,000, and 5,000 samples. Consistent hyperparameters were maintained while testing various training set sizes to investigate the influence of training sample size on validation error.

As expected, the smallest dataset of 10 samples resulted in the highest validation loss MAE, as depicted in the semi-logarithmic plot of Figure 9. The validation MAE decreased with increasing sample size, reaching its lowest with the 5,000-sample dataset. Smaller datasets, particularly those with 10 and 50 samples, exhibited variability in validation performance across iterations, indicating unreliable model performance and suggesting that such small sample sizes were unsuitable for use. However, datasets with more than 500 samples demonstrated better consistent performance, implying model reliability.

Table 5: Performance comparison of different graph construction of GraphParcelNet configurations

Model	Graph Construction		Training/Validation		Testing		Evaluation	
	Time (s)	Memory (MB)	Time (s)	Memory (MB)	Time (s)	Memory (MB)	MAE	MSE
Vector Domain								
1. GraphParcelNet (Delaunay)	132.20	1254.69	33.81	1127.00	0.07	1166.72	0.0548	0.0070
2. GraphParcelNet (10 Nearest Neighbors)	134.09	1229.54	64.18	1358.91	0.20	1476.41	0.0570	0.0076
3. GraphParcelNet (20 Nearest Neighbors)	134.38	1240.91	107.53	1214.88	0.36	1426.82	0.0563	0.0073
4. GraphParcelNet (100 Nearest Neighbors)	141.10	1380.72	434.13	1423.29	1.53	1400.41	0.0608	0.0084
Raster Domain								
Pixel Classification [25]	-	-	36000	-	439200	-	-	-

Table 6: Hyperparameters and their tested values.

Hyperparameter	Values
Learning Rate	0.001, 0.0001, 0.00001
Number of Layers	1, 2, 3, 4
Hidden dimension	32, 64, 128
Dropout Rate	0.5, 0.8
Weight Decay	0.00001
Number of Maximum Epochs	4000

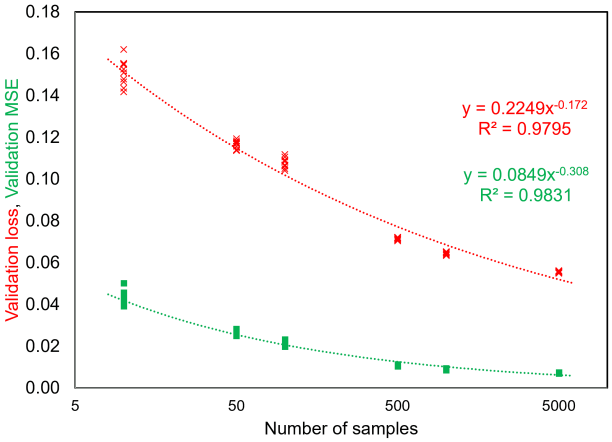

Figure 9: Validation MAE and MSE as a function of the number of training samples.

The validation loss and MSE trendlines showed a negative power function relationship with the number of training samples, indicating diminishing returns with increasing sample size. When considering validation MAE and MSE for 500, 1,000, and 5,000 samples, the difference between 500 and 5,000 was slight. The MAE and MSE for 500 samples were 0.0715 and 0.0110, respectively, while for 5,000 samples, they were 0.0548 and 0.0070. This corresponds to only a 0.0167 and 0.004 increase in error for the 500-sample dataset. Given that the effort to collect ground truth values is reduced tenfold. The number of training samples should be considered an acceptable trade-off between effort and accuracy, depending on the desired estimated error and available resources.

5 Conclusion

GraphParcelNet provides a novel solution for estimating parcel-level impervious surface ratios by utilizing Delaunay triangulation to construct graphs from land parcel centroids, incorporating various spectral indices and demographic characteristics as node features. The study explored alternative graph construction methods, such as K-nearest neighbors, to evaluate their impact on model performance. While increasing the number of neighbors improved the model's ability to capture spatial relationships, it also significantly increased computational time and memory usage. The results demonstrated the efficacy of GraphParcelNet in predicting parcel-level impervious surface ratios using geospatial vector data regression, outperforming other regression models such as CatBoost, MLP, SVR, and TabNet.

Furthermore, the impact of training sample size on regression accuracy was assessed, showing that larger training datasets generally led to improved model performance. However, diminishing returns were observed beyond a certain range, suggesting the need to balance dataset size and labeling process time. GraphParcelNet's ability to process large-scale geospatial data with lower computational requirements makes it a practical alternative to recent pixel-based classification methods. Future research could explore applying this framework to other geospatial regression tasks, further expanding its utility in urban analytics and geospatial data science.

6 Acknowledgements

This work was supported by the National Science Foundation (NSF) under grants 2050986 and 2318641 and the National Aeronautics and Space Administration (NASA) under grant 80NSSC22K1670 to Texas A&M University-Corpus Christi. Any opinions, findings, conclusions, or recommendations expressed in this material are those of the authors and do not necessarily reflect the views of NSF and NASA. We thank Hannah Garcia for assembling the demographic data and Aaliyah Timms for estimating the ground truth data. We thank Icograms (icograms.com) for providing services and materials in developing Figure 1.

References

[1] Jesus Aguirre-Gutiérrez, Arie C. Seijmonsbergen, and Joost F. Duivenvoorden. 2012. Optimizing land cover classification accuracy for change detection, a combined pixel-based and object-based approach in a mountainous area in Mexico. *Applied Geography* 34 (2012), 29–37. https://doi.org/10.1016/j.apgeog.2011.10.010

[2] Sercan O. Arik and Tomas Pfister. 2020. TabNet: Attentive interpretable tabular learning. arXiv:1908.07442 [cs.LG] https://arxiv.org/abs/1908.07442

[3] Franz Aurenhammer, Rolf Klein, and Der-Tsai Lee. 2013. *Voronoi Diagrams and Delaunay Triangulations.* WORLD SCIENTIFIC. https://doi.org/10.1142/8685 arXiv:https://worldscientific.com/doi/pdf/10.1142/8685

[4] Rebekka Burkholz, John Quackenbush, and Daniel Bojar. 2021. Using graph convolutional neural networks to learn a representation for glycans. *Cell Reports* 35, 11 (June 2021). https://doi.org/10.1016/j.celrep.2021.109251

[5] Bo cai Gao. 1996. NDWI—A normalized difference water index for remote sensing of vegetation liquid water from space. *Remote Sensing of Environment* 58, 3 (1996), 257–266. https://doi.org/10.1016/S0034-4257(96)00067-3

[6] Ugyen Jigten Dorji, Anon Plangprasopchok, Navaporn Surasvadi, and Chaiyaphum Siripanpornchana. 2019. A machine learning approach to estimate median income levels of sub-districts in Thailand using satellite and geospatial data. In *Proceedings of the 3rd ACM SIGSPATIAL International Workshop on AI for Geographic Knowledge Discovery.* 11–14. https://doi.org/10.1145/3356471.3365230

[7] Andrea Gemelli, Dasara Shullani, Daniele Baracchi, Simone Marinai, and Alessandro Piva. 2024. Structure matters: Analyzing videos via graph neural networks for social media platform attribution. In *2024 IEEE International Conference on Acoustics, Speech and Signal Processing (ICASSP).* 4735–4739. https://doi.org/10.1109/ICASSP48485.2024.10447089

[8] Anatoly A. Gitelson, Yoram J. Kaufman, Robert Stark, and Don Rundquist. 2002. Novel algorithms for remote estimation of vegetation fraction. *Remote Sensing of Environment* 80, 1 (2002), 76–87. https://doi.org/10.1016/S0034-4257(01)00289-9

[9] Driss Haboudane, John R. Miller, Elizabeth Pattey, Pablo J. Zarco-Tejada, and Ian B. Strachan. 2004. Hyperspectral vegetation indices and novel algorithms for predicting green LAI of crop canopies: Modeling and validation in the context of precision agriculture. *Remote Sensing of Environment* 90, 3 (2004), 337–352. https://doi.org/10.1016/j.rse.2003.12.013

[10] Fenghua Huang, Ying Yu, and Tinghao Feng. 2019. Automatic extraction of impervious surfaces from high resolution remote sensing images based on deep learning. *Journal of Visual Communication and Image Representation* 58 (Jan. 2019), 453–461. https://doi.org/10.1016/j.jvcir.2018.11.041

[11] Sha Huang, Lina Tang, Joseph P. Hupy, Yang Wang, and Guofan Shao. 2021. A commentary review on the use of normalized difference vegetation index (NDVI) in the era of popular remote sensing. *Journal of Forestry Research* 32, 1 (2021), 1–6. https://doi.org/10.1007/s11676-020-01155-1

[12] Bo Hui, Da Yan, Wei-Shinn Ku, and Wenlu Wang. 2020. Predicting economic growth by region embedding: A multigraph convolutional network approach. In *Proceedings of the 29th ACM International Conference on Information & Knowledge Management.* 555–564. https://doi.org/10.1145/3340531.3411882

[13] David B. Jennings, S. Terrence Slonecker, and Donald Garofalo. 2001. Remote sensing of impervious surfaces: A review. *Remote Sensing Reviews* 20, 3 (2001), 227–255. https://doi.org/10.1080/02757250109532436

[14] Reza Khatami, Giorgos Mountrakis, and Stephen V. Stehman. 2016. A meta-analysis of remote sensing research on supervised pixel-based land-cover image classification processes: General guidelines for practitioners and future research. *Remote Sensing of Environment* 177 (2016), 89–100. https://doi.org/10.1016/j.rse.2016.02.028

[15] Konstantin Klemmer, Nathan Safir, and Daniel B. Neill. 2023. Positional encoder graph neural networks for geographic data. arXiv:2111.10144 [cs.LG] https://arxiv.org/abs/2111.10144

[16] Jim Lee, Hua Zhang, and Yuxia Huang. 2024. Toward a more socially equitable stormwater management fee: The case of Corpus Christi in Texas, USA. *Environment and Planning B: Urban Analytics and City Science* 51, 4 (May 2024), 939–953. https://doi.org/10.1177/23998083231207535

[17] Kexuan Li, Jun Zhu, Anthony R. Ives, Volker C. Radeloff, and Fangfang Wang. 2023. Semiparametric regression for spatial data via deep learning. *Spatial Statistics* 57 (2023), 100777. https://doi.org/10.1016/j.spasta.2023.100777

[18] Christopher Morris, Martin Ritzert, Matthias Fey, William L. Hamilton, Jan Eric Lenssen, Gaurav Rattan, and Martin Grohe. 2019. Weisfeiler and Leman go neural: Higher-order graph neural networks. In *Proceedings of the AAAI Conference on Artificial Intelligence*, Vol. 33. 4602–4609. https://doi.org/10.1609/aaai.v33i01.33014602

[19] Fabian Pedregosa, Gaël Varoquaux, Alexandre Gramfort, Vincent Michel, Bertrand Thirion, Olivier Grisel, Mathieu Blondel, Peter Prettenhofer, Ron Weiss, Vincent Dubourg, Jake Vanderplas, Alexandre Passos, David Cournapeau, Matthieu Brucher, Matthieu Perrot, and Édouard Duchesnay. 2011. Scikit-learn: Machine learning in Python. *Journal of Machine Learning Research* 12 (2011), 2825–2830.

[20] Liudmila Prokhorenkova, Gleb Gusev, Aleksandr Vorobev, Anna Veronika Dorogush, and Andrey Gulin. 2019. CatBoost: unbiased boosting with categorical features. arXiv:1706.09516 [cs.LG] https://arxiv.org/abs/1706.09516

[21] Yossi Rubner, Carlo Tomasi, and Leonidas J. Guibas. 2000. The Earth Mover's Distance as a metric for image retrieval. , 99–121 pages. https://doi.org/10.1023/A:1026543900054

[22] Franco Scarselli, Marco Gori, Ah Chung Tsoi, Markus Hagenbuchner, and Gabriele Monfardini. 2009. The graph neural network model. *IEEE Transactions on Neural Networks* 20, 1 (Jan. 2009), 61–80. https://doi.org/10.1109/TNN.2008.2005605

[23] Michael A. Stephens. 1992. *Introduction to Kolmogorov (1933) On the empirical determination of a distribution.* Springer New York, 93–105. https://doi.org/10.1007/978-1-4612-4380-9_9

[24] Michael W. Strohbach, Dagmar Haase, and Nadja Kabisch. 2019. The "hidden urbanization": Trends of impervious surface in low-density housing developments and resulting impacts on the water balance. *Frontiers in Environmental Science* 7 (March 2019), 29. https://doi.org/10.3389/fenvs.2019.00029

[25] Lapone Techapinyawat, Aaliyah Timms, Jim Lee, Yuxia Huang, and Hua Zhang. 2024. Integrated urban land cover analysis using deep learning and post-classification correction. *Computer-Aided Civil and Infrastructure Engineering* (May 2024). https://doi.org/10.1111/mice.13277

[26] Texas Geographic Information Office. 2023. Land Parcels (shapefile/geodatabase). https://tnris.org/stratmap/land-parcels Accessed: 2024-03-12.

[27] Waldo R. Tobler. 1970. A computer movie simulating urban growth in the Detroit region. *Economic Geography* 46, sup1 (1970), 234–240. https://doi.org/10.2307/143141 arXiv:https://www.tandfonline.com/doi/pdf/10.2307/143141

[28] Xin-Yi Tong, Gui-Song Xia, Qikai Lu, Huanfeng Shen, Shengyang Li, Shucheng You, and Liangpei Zhang. 2020. Land-cover classification with high-resolution remote sensing images using transferable deep models. *Remote Sensing of Environment* 237 (2020), 111322. https://doi.org/10.1016/j.rse.2019.111322

[29] United States Environmental Protection Agency. 2023. EJSCREEN: Environmental Justice Screening and Mapping Tool. https://www.epa.gov/ejscreen Accessed: 2024-03-12.

[30] U.S. Census Bureau. 2022. American Community Survey. https://www.census.gov/programs-surveys/acs/ Accessed: 2024-03-12.

[31] Qihao Weng. 2012. Remote sensing of impervious surfaces in the urban areas: Requirements, methods, and trends. *Remote Sensing of Environment* 117 (2012), 34–49. https://doi.org/10.1016/j.rse.2011.02.030

[32] Wen Wu, Chunlin Li, Miao Liu, Yuanman Hu, and Chunliang Xiu. 2020. Change of impervious surface area and its impacts on urban landscape: An example of Shenyang between 2010 and 2017. *Ecosystem Health and Sustainability* 6, 1 (2020). https://doi.org/10.1080/20964129.2020.1767511

[33] Keyulu Xu, Weihua Hu, Jure Leskovec, and Stefanie Jegelka. 2019. How powerful are graph neural networks? arXiv:1810.00826 [cs.LG] https://arxiv.org/abs/1810.00826

[34] Jie Zhou, Ganqu Cui, Shengding Hu, Zhengyan Zhang, Cheng Yang, Zhiyuan Liu, Lifeng Wang, Changcheng Li, and Maosong Sun. 2020. Graph neural networks: A review of methods and applications. *AI Open* 1 (Jan. 2020), 57–81. https://doi.org/10.1016/j.aiopen.2021.01.001

[35] Di Zhu, Yu Liu, Xin Yao, and Manfred M. Fischer. 2022. Spatial regression graph convolutional neural networks: A deep learning paradigm for spatial multivariate distributions. *GeoInformatica* 26, 4 (Oct. 2022), 645–676. https://doi.org/10.1007/s10707-021-00454-x